



Nanofabrication of tungsten zone plates with integrated platinum central stop for hard X-ray applications



F. Uhlén^{a,*}, D. Nilsson^a, J. Rahomäki^a, L. Belova^b, C.G. Schroer^c, F. Seiboth^c, A. Holmberg^a, H.M. Hertz^a, U. Vogt^a

^a Department of Applied Physics, Royal Institute of Technology, SE-10691 Stockholm, Sweden

^b Department of Material Science Engineering, Royal Institute of Technology, SE-10691 Stockholm, Sweden

^c Institute of Structural Physics, Technische Universität Dresden, 01062 Dresden, Germany

ARTICLE INFO

Article history:

Received 14 September 2013

Accepted 17 October 2013

Available online 26 October 2013

Keywords:

X-ray diffractive optics

Zone plates

Tungsten

Platinum

Hard X-ray microscopy

Ptychography

ABSTRACT

We present a nanofabrication process for producing tungsten zone plates used in hard X-ray applications including a method of integrating a high-energy absorbing central stop with the optic. Tungsten zone plates are structured with electron-beam lithography and subsequent reactive ion etching. The central stop originates from a platinum wire. It is cut to dimension by focused ion beam etching, and afterwards attached to the zone plate center using ion beam induced deposition of platinum. A zone plate with integrated central stop will simplify alignment in hard X-ray scanning microscope arrangements where the 0th order light must be eliminated. The focusing performance of the zone plate device was investigated by scanning coherent diffraction imaging (ptychography) at 8 keV photon energy. We could demonstrate a diffraction-limited focus size of 53 nm diameter full-width-at-half-maximum. Tungsten zone plates with integrated central stops show promising results for use in hard X-ray microscopes at high-brightness facilities.

© 2013 Elsevier B.V. All rights reserved.

1. Introduction

The emergence of hard X-ray microscopy at high-brilliance X-ray sources has paved way for discoveries in diverse fields of science; from life sciences to materials engineering. The small wavelength and large penetrating power in combination with different contrast mechanisms of X-rays allow investigation of inner structures of specimens without extensive preparation measures, e.g., X-ray diffraction [1,2], absorption [3], and fluorescence [4].

Hard X-ray scanning microscopes depend on focusing optics which can produce an intense and well-defined nanobeam. The optics can either be based on diffraction, reflection or refraction. Fresnel zone plates (FZP) are a commonly used diffractive optical device. They consist of concentric circular zones with radially decreasing zone widths. Adjacent zones are alternating transparent and phase-shifting/absorbing. The outermost zone width determines the spatial resolution in X-ray microscopes employing FZP. Today, zone plate fabrication most commonly relies on electron-beam lithography (EBL). With this method, electron scattering in the electron-sensitive resist limits the smallest zone width attainable. State-of-the-art zone plate processes can reach zone widths down to 12 nm [5,6], although this is mainly limited to soft X-ray zone plates. Hard X-rays, however, require much thicker

optical material, e.g., tungsten [7], gold [8], iridium [9], or diamond [10], in order for the zone plate to focus efficiently, i.e., to have a high diffraction efficiency. For small zone widths this implies very high aspect-ratios, which are non-trivial to fabricate. Hence, the smallest zone width for hard X-ray FZPs are today limited to around 15–20 nm using EBL-based processes [9].

Hard X-ray scanning microscope arrangements require careful aligning of optical components, i.e., FZP, central stop, apertures, sample, and detectors, along the optical axis for the instrument to function satisfactorily. This step may be very time-consuming. Thus, combining compatible parts, e.g., FZP and central stop, would greatly simplify the arrangements. Unifying optics with micrometer-thick central stops has been successfully developed for soft X-ray applications [11,12]. However, for highly penetrating multi-keV X-rays the central stop needs to be tens of micrometers thick and of high-Z material in order to absorb a sufficient amount of radiation.

In this paper we present a new method of mounting a highly absorbing central stop for hard X-rays in the center of a FZP and demonstrate the performance at 8 keV photon energy. To characterize the optical device, scanning coherent diffraction microscopy, or so-called ptychography, was performed by scanning a highly scattering test sample across the FZP-focused beam and recording the far-field diffraction pattern. Doing so provides both the complex illumination on the sample and its transmission function [13]. By propagating the reconstructed complex illumination to

* Corresponding author. Tel.: +46 855378113.

E-mail address: fredrik.uhlen@biox.kth.se (F. Uhlén).

the optic and focus, respectively, complete wave-field characterization is obtained, i.e., aberrations in the optic, focus spot size, and full caustic of the beam [14–16].

2. Methods

2.1. Nanofabrication of tungsten zone plate

The nanofabrication process is based on a tri-layer material stack prepared onto a thick diamond substrate; see Fig. 1(a). The zone plate pattern is defined by EBL (Fig. 1(b)) and subsequently transferred into the material stack via reactive ion etching (RIE) (Fig. 1(c)–(d)). In the final step a thick central stop is integrated with the optic by attaching a piece of thick platinum wire via ion-beam methods (Fig. 1(e)). Below follows a more detailed description of the process.

The process starts by sputter-depositing 1 μm of tungsten onto a 100 μm CVD diamond substrate (Diamond Materials GmbH). The sputtering is performed in an AJA Orion system in dc magnetron configuration with following parameters: 25 sccm Ar gas flow, 5 mTorr pressure, 150 W power, 250 $^{\circ}\text{C}$ sample temperature, and with a deposition rate of 11 nm/min. These parameters have been optimized for low stress in order to obtain thick tungsten films. Nevertheless, the film also becomes columnar with large grain size, which limits the smallest zone width that can be reliably etched into the tungsten [17]. Onto the tungsten, a 30 nm chromium hardmask is electron-beam evaporated. This step is performed in an in-house system (Eurovac) at a low base-pressure (10^{-8} mbar). In the final preparation step, 100 nm of electron-beam resist (Zep 7000, Zeon Chemicals L.P.) is spin-coated on the material stack and baked at 170 $^{\circ}\text{C}$ for 30 min in a convection oven. To define the zone plate pattern, the resist is patterned by an EBL system (Raith 150 system). Exposure is performed at 25 kV and with a standard dose of 100 $\mu\text{C}/\text{cm}^2$. After exposure, the pattern is developed in hexylacetate for 30 s, and then rinsed in isopropanol and pentane (Fig. 1(b)). To transfer the zone plate pattern from the resist to the underlying chromium and tungsten, two separate RIE steps (Oxford Instruments, Plasmalab 100 system) are performed. The chromium is etched with Cl_2 and O_2 at 8 and 2 sccm gas flows, respectively, 20 mTorr pressure, 10 W RF power, 10 W inductively coupled plasma (ICP) power, 20 $^{\circ}\text{C}$ sample temperature, and an etch-rate of 2.9 nm/min (Fig. 1(c)). Using the chromium template as hardmask, the tungsten is etched with SF_6 and O_2 at 8 and 2 sccm gas flows, respectively, 10 mTorr pressure, 40 W RF power, -20 $^{\circ}\text{C}$ sample temperature, and an etch-rate of 28 nm/min (Fig. 1(d)). The etching is anisotropic and is capable of producing

high-aspect-ratio tungsten nanostructures [10]. Still there is an issue of linewidth-dependent etching-rate, i.e., outermost zones are not as deeply etched as those close to the zone plate center. The fabricated zone plate has a diameter of 75 μm , outermost zone width of 50 nm, and a first-order focal length of 25 mm at 8 keV photon energy. For zone plate characterization (see Section 3.1), a 600 nm thick tungsten test sample of consisting of a matrix with Siemens stars was also fabricated in the same way.

2.2. Integrating the platinum central stop

The process of integrating a central stop with the nanostructured zone plate lens is demonstrated in Fig. 2. This work is conducted in an FEI Nova 600 Nanolab dual beam system. The system combines a scanning electron microscope (SEM) with focused ion beam (FIB) technologies together with different gas chemistries. A micromanipulator is also positioned in the system. The micromanipulator is brought in contact with a 25 μm diameter platinum wire (Goodfellow Cambridge Limited) and soldered together with platinum using ion beam induced deposition (IBID). Platinum is deposited using 30 keV gallium ions at 300 pA beam current together with a platinum precursor gas. The wire is then chopped by the FIB at high ion current. Due to severe redeposition when milling through the thick wire, a wide milling cut is required (Fig. 2(a)). FIB milling is performed at 30 kV and 20 nA beam current. The shortened wire is then polished by the FIB to a length of 25 μm (Fig. 2(b)). The platinum wire is brought by the micromanipulator to the zone plate center and joined together with platinum using IBID (Fig. 2(c)–(d)). A difficulty in this step is that platinum deposition has to be done from the top, while the sealing point is at the bottom of the thick wire which partially blocks the beam and the precursor flow. In order to ensure good mechanically solid soldering some platinum deposition overlaps onto undesired parts of the zone plate. However, since this layer is very thin and has a low density of platinum (the resulting platinum deposit contains approximately 23 at.% Pt, 8 at.% Ga, the rest being carbon from the precursor that is not fully decomposed), the zone plate is only negligibly affected. In the last step the micromanipulator is detached from the platinum wire with the FIB. A final device is shown in Fig. 3.

Ideally, the wire should be placed standing up. In this way the absorption through the wire would be the same over the whole central stop. For 25 μm platinum, the X-ray transmission at 8 keV is only 2.6×10^{-5} . However, the geometry of the system and limitations in the micromanipulator stage movements render it much less difficult to position the wire laying down. This

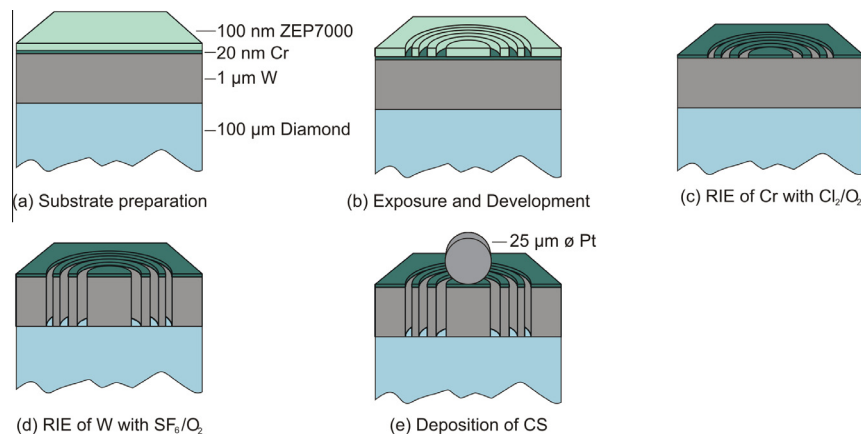


Fig. 1. Nanofabrication process: (a) material stack, (b) electron-beam exposure and subsequent development, (c) reactive-ion-etching of chromium using a chlorine-based plasma, (d) reactive-ion-etching of tungsten using a sulfur-hexafluoride-based plasma, (e) soldering of central stop (CS) on zone plate using IBID.

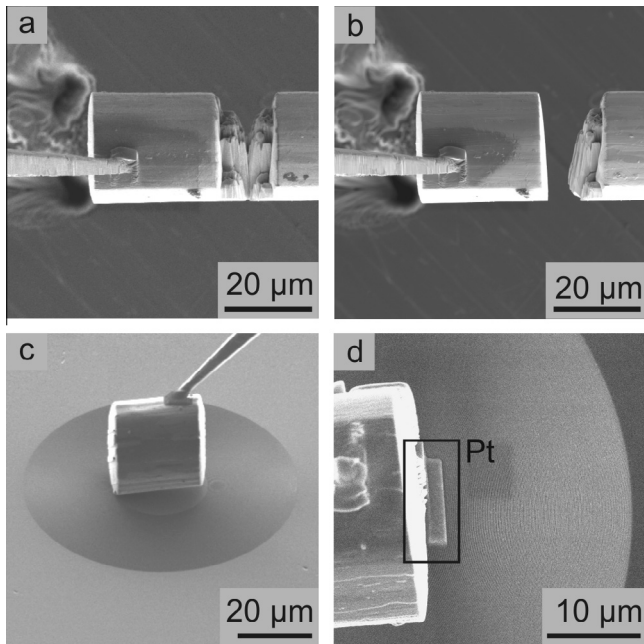


Fig. 2. Soldering of central stop: (a) FIB-milling of platinum wire, (b) polishing of cut surface, (c) fixation of wire to zone plate, (d) soldering with platinum (marked with a rectangle).

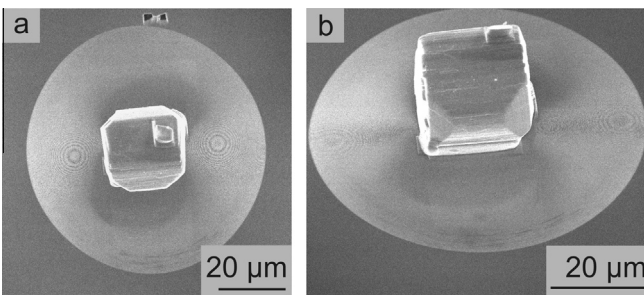


Fig. 3. Zone plate with integrated central stop: (a) top-view, (b) 45 degrees tilt angle.

arrangement results in an increasing X-ray transmission further out on two sides of the central stop. The X-ray transmission and thickness of the central stop in cross-section is demonstrated in Fig. 4. From -10 to $10 \mu\text{m}$ the transmission is less than 2×10^{-3} . Hence the central stop is considered very efficient within this region.

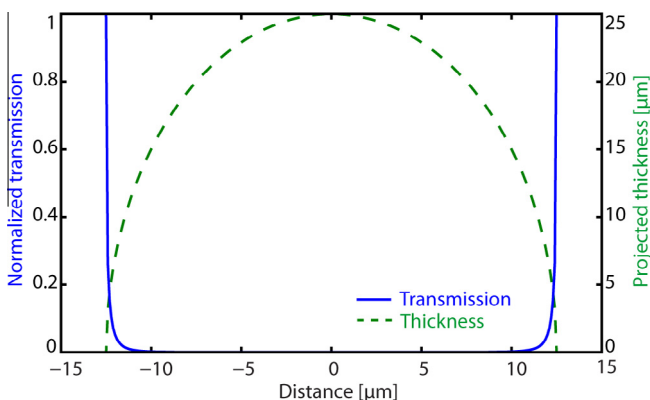


Fig. 4. X-ray transmission and thickness through the platinum central stop.

3. Zone plate characterization using ptychography

Wave-field characterization in terms of scanning coherent diffraction microscopy, ptychography, was performed at beamline P06 at the synchrotron radiation source PETRA III at DESY in Hamburg, Germany. An undulator in combination with Si-crystal monochromator delivers hard X-rays with tunable energy in the range from 2.4 to 100 keV. For the experiment described in this section, 8 keV photon energy was used. The X-rays travel downstream to a scanning microscope setup, consisting of nanofocusing optic, sample stage, and detectors. The zone plate optic was coherently illuminated allowing ptychographic experiments [1,14]. A $10 \mu\text{m}$ -diameter order sorting aperture (OSA) was used to single out the first-order focus. Approximately in the focal plane, 25 mm behind the zone plate, a tungsten test sample with Siemens stars was placed on a scanning unit. The sample was scanned in a raster fashion over a $1.2 \mu\text{m} \times 0.8 \mu\text{m}$ area with 20 nm steps perpendicular to the optical axis. A far-field diffraction pattern was recorded at each position by a diffraction camera (Pilatus 300 K). The ptychographic data set then served as input to an iterative algorithm in order to reconstruct the object's transmission function as well as the complex wave-field at the sample position [13,18]. Fig. 5 shows the reconstructed object phase.

By propagating the wave-field along the optical axis full characterization of the zone plate was obtained. Fig. 6(a) demonstrates the phase error from a perfectly spherical wave just behind the zone plate. Ideally, the phase error should be the same everywhere. However, the foci of the horizontal and vertical caustic coincide, indicating that the optic does not suffer from any severe astigmatism, see Fig. 7(a) and (b). Furthermore, propagating the wave-field to the focal plane yields Fig. 6(b). The focus has a full-width-at-half-maximum (FWHM) of 53 nm in diameter, which agrees well with a diffraction-limited zone plate with 50 nm outermost zone width.

The diffraction efficiency was measured at 9.25 keV photon energy with an in-house liquid-metal-jet hard X-ray source together with a CCD-detector. The measurement gave a diffraction efficiency of 2.1%.

4. Conclusion and outlook

In this paper we have presented a nanofabrication process for producing tungsten zone plates with 50 nm outermost zone width. Furthermore, a new method for mounting a highly efficient

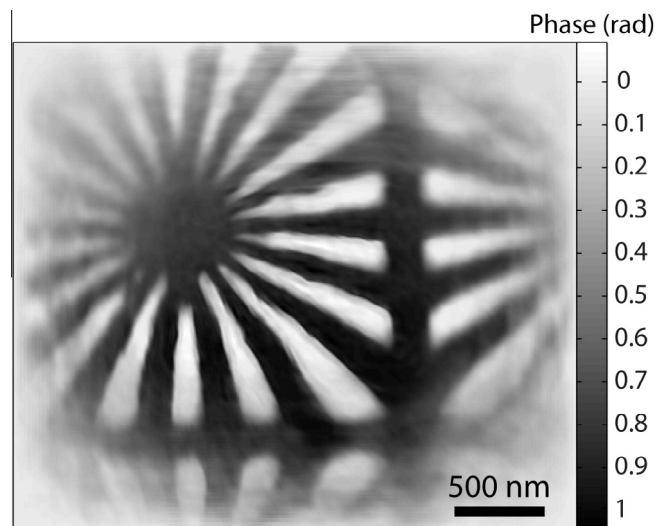


Fig. 5. Reconstructed object phase.

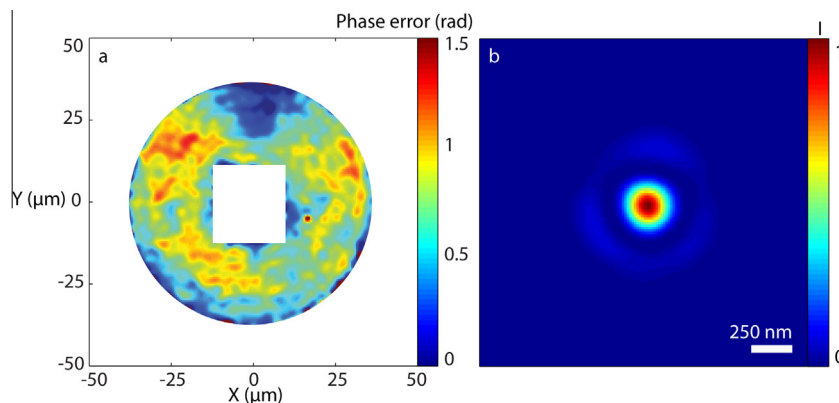


Fig. 6. (a) Phase error from a perfectly spherical wave just behind zone plate, (b) relative intensity (absolute square of wave-field) in the focal plane.

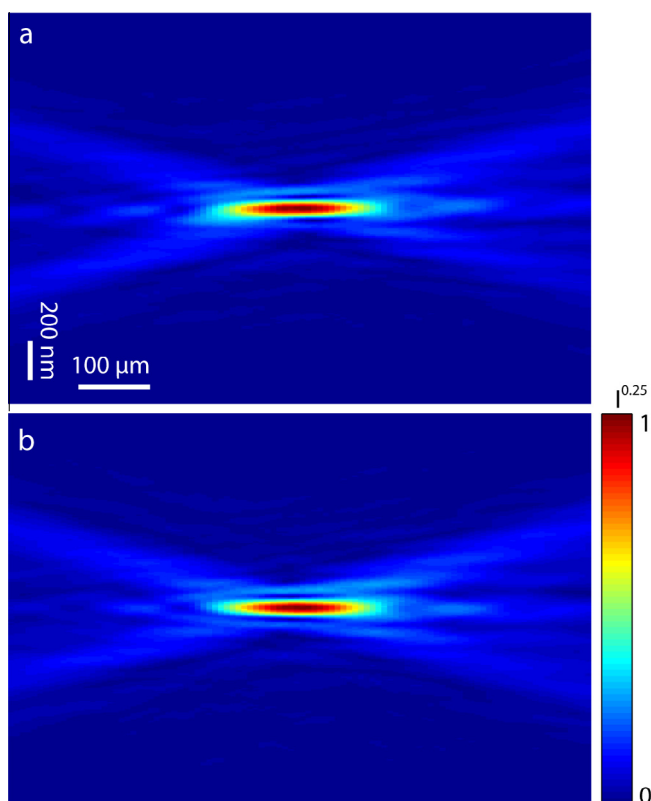


Fig. 7. Horizontal (a) and vertical (b) caustic of the square root of the absolute wave-field (fourth root of the intensity). The square root is performed to make the caustic form more visible.

platinum central stop directly on the optic has also been demonstrated. The combined optic and central stop will facilitate simple alignment of the optic in hard X-ray experimental arrangements. The diffractive optical device has been characterized with ptychography. Results showed that the optic is diffraction-limited and a focus spot size of 53 nm was found. A measured diffraction efficiency of 2.1% was, however, low and improved fabrication of high aspect ratios for small zone widths is crucial.

Acknowledgements

The authors gratefully acknowledge the financial support of the Swedish Science Research Council, the Swedish Foundation for

Strategic Research, the Göran Gustafsson Foundation, the Wallenberg Foundation, and the European Community's Seventh Framework Programme (FP7/2007–2013) under Grant No. 226716. The experiment was performed at the Hard X-ray Micro/Nano-Probe beamline P06 at PETRA III (DESY) in Hamburg-Bahrenfeld.

References

- [1] C.G. Schroer, P. Boye, J.M. Feldkamp, J. Patommel, D. Samberg, A. Schropp, A. Schwab, S. Stephan, G. Falkenberg, G. Wellenreuther, N. Reimers, Nucl. Instrum. Methods A 616 (2–3) (2010) 93–97.
- [2] H.N. Chapman, P. Fromme, A. Barty, T.A. White, R.A. Kirian, A. Aquila, M.S. Hunter, J. Schulz, D.P. DePonte, U. Weierstall, R.B. Doak, F.R.N.C. Maia, A.V. Martin, I. Schlichting, L. Lomb, N. Coppola, R.L. Shoeman, S.W. Epp, R. Hartmann, D. Rolles, A. Rudenko, L. Foucar, N. Kimmel, G. Weidenspointner, P. Holl, M. Liang, M. Barthelmeß, C. Caleman, S. Boutet, M.J. Bogan, J. Krzywinski, C. Bostedt, S. Bajt, L. Gumprecht, B. Rudek, B. Erk, C. Schmidt, A. Hömke, C. Reich, D. Pietschner, L. Strüder, G. Hauser, H. Gorke, J. Ullrich, S. Herrmann, G. Schaller, F. Schopper, H. Soltau, K.-U. Kühnel, M. Messerschmidt, J.D. Bozek, S.P. Hau-Riege, M. Frank, C.Y. Hampton, R.G. Sierra, D. Starodub, G.J. Williams, J. Hajdu, N. Timneanu, M.M. Seibert, J. Andreasson, A. Rocker, O. Jönsson, M. Svenda, S. Stern, K. Nass, R. Andritschke, C.-D. Schröter, F. Krasniqi, M. Bött, K.E. Schmidt, X. Wang, I. Grotjohann, J.M. Holton, T.R.M. Barends, R. Neutze, S. Marchesini, R. Fromme, S. Schorb, D. Rupp, M. Adolph, T. Gorkhovei, I. Andersson, H. Hirsemann, G. Potdevin, H. Graafsma, B. Nilsson, J.C.H. Spence, Nature 470 (7332) (2011) 73–77.
- [3] C. Bressler, M. Chergui, Annu. Rev. Phys. Chem. 61 (2010) 263–274.
- [4] S. Bohic, A. Simionovici, A. Snigirev, R. Ortega, G. Devès, Appl. Phys. Lett. 78 (2001) 3544–3546.
- [5] J. Reinspach, F. Uhlén, H.M. Hertz, A. Holmberg, J. Vac. Sci. Technol. B 29 (6) (2011) 06FG02.
- [6] W. Chao, J. Kim, S. Rekawa, P. Fischer, E.H. Anderson, Opt. Express 17 (20) (2009) 17669–17677.
- [7] P. Charalambous, I. McNulty, C. Eyberger, B. Lai, AIP Conf. Proc. 65 (1) (2011) 65–68.
- [8] Y. Feng, M. Feser, A. Lyon, S. Rishton, X. Zeng, S. Chen, S. Sassolini, W. Yun, J. Vac. Sci. Technol. B 25 (6) (2007) 2004–2007.
- [9] J. Vila-Comamala, S. Gorelick, E. Färm, C.M. Kewish, A. Diaz, R. Barrett, Opt. Express 19 (1) (2011) 175–184.
- [10] F. Uhlén, S. Lindqvist, D. Nilsson, J. Reinspach, U. Vogt, H.M. Hertz, A. Holmberg, R. Barrett, J. Vac. Sci. Technol. B 29 (6) (2011) 06FG03.
- [11] P. Charalambous, Microscopy (2004) 127–129.
- [12] J. Vila-Comamala, K. Jefimovs, J. Raabe, T. Pilvi, R.H. Fink, M. Senoner, A. Maassdorf, M. Ritala, C. David, Ultramicroscopy 109 (11) (2009) 1360–1364.
- [13] P. Thibault, M. Dierolf, A. Menzel, O. Bunk, C. David, F. Pfeiffer, Science 321 (5887) (Jul. 2008) 379–382.
- [14] C.G. Schroer, H. Susanne, A. Goldschmidt, R. Hoppe, J. Patommel, D. Samberg, A. Schropp, F. Seiboth, S. Stephan, S. Sch, M. Burghammer, M. Denecke, G. Wellenreuther, G. Falkenberg, Proc. SPIE Int. Soc. Opt. Eng. 8141 (2011) 814103-1–814103-10.
- [15] A. Schropp, P. Boye, J.M. Feldkamp, R. Hoppe, J. Patommel, D. Samberg, S. Stephan, K. Giewekemeyer, R.N. Wilke, T. Salditt, J. Gulden, A.P. Mancuso, I.A. Vartanyants, E. Weckert, S. Schöder, M. Burghammer, C.G. Schroer, Appl. Phys. Lett. 96 (9) (2010) 091102.
- [16] J. Vila-Comamala, A. Diaz, M. Guizar-Sicairos, A. Manton, C.M. Kewish, A. Menzel, O. Bunk, C. David, Opt. Express 19 (22) (2011) 21333–21344.
- [17] P. Charalambous, AIP Conf. Proc. 507 (2000) 625–630.
- [18] A.M. Maiden, J.M. Rodenburg, Ultramicroscopy 109 (10) (Sep. 2009) 1256–1262.